Two-dimensional Rayleigh model for bubble evolution in soft tissue

Menahem Friedman and Moshe Strauss
Nuclear Research Center, Negev, P.O. Box 9001, Beer Sheva, Israel

Peter Amendt and Richard A. London
Lawrence Livermore National Laboratory, Livermore, California 94550

Michael E. Glinsky
BHP Petroleum, Houston, Texas 77056

(Received 25 April 2001; accepted 13 February 2002; published 8 April 2002)

The understanding of vapor bubble generation in a soft tissue near a fiber-optic tip has in the past required two-dimensional (2D) hydrodynamic simulations. For 1D spherical bubble expansions a simplified and useful Rayleigh-type model can be applied. For 2D bubble evolution, such a model has not been developed. In this work we develop a Rayleigh-type model for 2D bubble expansion that is much faster and simpler than 2D hydrodynamic simulations and can be applied toward the design and understanding of fiber-based medical therapies. The model is based on a flow potential representation of the hydrodynamic motion and is described by a Laplace equation with a moving boundary condition at the bubble surface. In order for the Rayleigh-type 2D model to approximate bubble evolution in soft tissue, we include viscosity and surface tension in the fluid description. We show that the 1D Rayleigh equation is a special case of our model. The Laplace equation is solved for each time step by a finite-element solver using a fast triangular unstructured mesh generator. Our simulations include features of bubble evolution as seen in experiments and are in good agreement with 2D hydrodynamic simulations. © *2002 American Institute of Physics.*
[DOI: 10.1063/1.1467654]

I. INTRODUCTION

In many medical therapies, bubbles are generated by short pulses of laser light delivered through an optical fiber.[1–4] Vapor bubbles are widely applied to cutting and breaking up of tissue by the generation of acoustic waves and by bubble expansion and collapse. For example, bubbles are used in laser-assisted coronary angioplasty for dissolving blood clots, in ophthalmology and dermatology for removing melanin structures, and in intraocular surgery for photodisrupting tissue.[1] Vapor bubble research in 1D and 2D has a long history in a variety of applications, in relation to bubble expansion and collapse far from boundaries and next to free and rigid boundaries.[5–11]

A theoretical description of the bubble evolution requires two-dimensional (2D) hydrodynamic simulations and therefore sophisticated computational capabilities.[2–4] For 1D spherically symmetric bubble evolution there exists a simplified treatment, based on an extended Rayleigh model, which is represented by an ordinary differential equation that can be easily solved.[5,6] For 2D bubble effects such as those created by the presence of a cylindrically symmetric fiber optic, such a treatment does not yet exist.

In this work we develop a 2D Rayleigh-type model which can be applied toward several medical applications. In order to simulate bubble evolution in soft tissue problems, we have extended the model to include viscosity and surface tension. Adding viscosity and surface tension also contributes to the stability of the numerical procedure. The proposed method is two-to-three orders of magnitude faster and requires an order of magnitude fewer spatial zones than the 2D compressible hydrodynamic simulations.

Our model is based on introducing a flow potential ϕ which is a solution of Laplace's equation.[7] The fluid velocity outside the bubble is $\mathbf{u}=-\nabla\phi$. This model is valid throughout most of the bubble's expansion and collapse phases since the fluid outside the bubble is incompressible, and irrotational to a good approximation.[8] A flow potential method was applied in previous work to treat cavities near and far from boundaries, using finite difference and boundary integral methods.[9–11] In this work we apply a general dynamic finite-element code which was designed for solving 2D elliptic partial differential equations over an arbitrary bounded domain with moving boundary conditions. The code provides detailed information throughout the fluid domain. It allows up to fourth-order polynomial approximations over the generated mesh. However, we found that second order was sufficient to obtain accurate and smooth solutions. As in the Rayleigh model, we assume that the inside of the bubble is uniform in pressure and density and we derive a moving boundary condition for ϕ at the bubble boundary. For the limiting 1D case, our model reduces to the known 1D Rayleigh model. For the general case we solve a Laplace's equation in cylindrical geometry with Dirichlet (specified ϕ) and homogeneous Neumann (specified normal component: $\partial\phi/\partial n=0$) boundary conditions applied to the moving bubble boundary. Dirichlet boundary conditions are applied on the bubble boundary and at infinity, where we set $\phi=0$. The homogeneous Neumann boundary conditions are applied on the fiber boundary and on the axis of symmetry,

where the normal flow velocity is zero. For every time step an unstructured mesh finite-element solver (UMFES) is used to update the triangulation of the region outside the bubble.[12,13]

Application of the model assumes an instantaneous deposition of laser energy in an aqueous system at the tip of a fiber. We obtained solutions in agreement with detailed hydrodynamic calculations and consistent with experimental characteristics of the expansion and the collapse of the bubble away from the fiber.[3,14]

The 2D Rayleigh-type model presented in this work, which includes viscosity and surface tension, can be applied toward the design and understanding of fiber-based medical therapies in more realistic geometries. The flow potential method can be extended to include other physical mechanisms that affect tissue behavior, including strength and failure properties. These mechanisms were treated successfully by the 1D Rayleigh model and the results were in agreement with 1D hydrodynamic simulations.[4] We believe that the same can be done possibly in the 2D Rayleigh case.

The plan of the paper is as follows: In Sec. II we discuss the physical model. The numerical procedure is represented in Sec. III. Computational results and discussion are given in Sec. IV and concluding remarks in Sec. V.

II. THE PHYSICAL MODEL

We first consider a vapor bubble generated in water by a short-pulse laser depositing energy near a fiber tip. Later, the effects of viscosity and surface tension will be added. Understanding the subsequent bubble evolution requires cylindrically symmetric 2D simulations or analysis.[3,15] We assume that the bubble interior is uniform in pressure as in a Rayleigh model, and that it evolves adiabatically with entropy S_0. After applying an equation of state (EOS) within the bubble, any of the quantities p (pressure), ρ (density), T (temperature), or ε (specific energy) together with S_0 will determine the remaining quantities.

A. Vapor bubble generation in water

For the region outside the bubble, the relevant hydrodynamic equations are the continuity equation

$$\frac{\partial \rho}{\partial t}+\nabla\cdot(\rho\mathbf{u})=0, \tag{1}$$

and the momentum equation

$$\frac{\partial \mathbf{u}}{\partial t}+\mathbf{u}\cdot\nabla\mathbf{u}=-\frac{\nabla p}{\rho}, \tag{2}$$

where ρ, p, $\mathbf{u}$ denote the density, pressure, and velocity of the fluid outside the bubble, respectively.

We assume a flow potential ϕ such that $\mathbf{u}=-\nabla\phi$. Consequently, we may integrate Eq. (2) from $\mathbf{r}$ to ∞ and obtain, independently of the bubble boundary trajectory

$$-\frac{\partial \phi}{\partial t}+\frac{1}{2}(\nabla\phi)^2=h(\infty)-h(\mathbf{r}), \tag{3}$$

where

$$dh=-dp/\rho, \quad h(\infty)-h(\mathbf{r})=\int_{\mathbf{r}}^{\infty}\frac{dp}{\rho}, \tag{4}$$

where $h(\mathbf{r})$ is the enthalpy at $\mathbf{r}$, and $h(\infty)$ is the ambient enthalpy at large $\mathbf{r}$.

For many cases of interest $\rho\approx$constant, i.e., we may replace $h(\infty)-h(\mathbf{r})$ in Eq. (4) by $(p(\infty)-p(\mathbf{r}))/\rho$ and get

$$\frac{d\phi}{dt}=\frac{p-p_\infty}{\rho}-\frac{u^2}{2}, \tag{5}$$

where $d/dt=(\partial/\partial t)+\mathbf{u}\cdot\nabla$, p is the pressure at $\mathbf{r}$, and p_∞ is the ambient pressure. Let θ parametrize the distance along the bubble boundary. Then, by enforcing Eq. (5) at the bubble boundary, we get

$$\frac{d\Phi(\theta)}{dt}=\frac{P-p_\infty}{\rho}-\frac{U^2(\theta)}{2}, \tag{6}$$

i.e., a relation between the pressure P, velocity $U(\theta)$, and the flow potential $\Phi(\theta)$, along the boundary. Equation (6) represents the boundary condition for the bubble expansion.

For incompressible flow, we may substitute $\rho\approx$constant in Eq. (1), and by using $\mathbf{u}=-\nabla\phi$ we obtain a Laplace equation for the region outside the bubble, i.e.,

$$\nabla^2\phi=0. \tag{7}$$

The solution of Eq. (7), along with the moving boundary condition, Eq. (6), represents the main ingredients of our 2D time-dependent bubble model. In the following, we assume that the boundary pressure P is the pressure p_b inside the bubble at all times.

We can show that Eqs. (6) and (7) are consistent with the 1D Rayleigh equation. For the 1D spherical case the solution of Eq. (7) is $\phi=C/r$. Using $u=-\partial\phi/\partial r$, we get $\phi=R^2U/r$. Inserting ϕ in Eq. (5) and evaluating on the bubble boundary ($r=R$), we get

$$R\ddot{R}+\frac{3}{2}U^2=\frac{P-p_\infty}{\rho}, \tag{8}$$

which is the 1D Rayleigh equation.[6]

By assuming $\rho\approx$constant, we have so far ignored the acoustic emission outside the bubble. However, the acoustic emission for a laser depositing its energy close to the fiber tip can be easily approximated. The acoustic wave is emitted on a short time scale relative to the bubble expansion. The initial bubble velocity perpendicular to the fiber tip for a uniform laser deposition is[16]

$$u_s=p_0/(2\rho c_s), \tag{9a}$$

where c_s is the adiabatic sound speed in water ($c_s=1.5\cdot10^5$ cm/s), p_0 is the initial bubble pressure, and ρ is the density outside the bubble. The acoustic energy emitted from the bubble equals the work done by the expanding bubble $e_s=\int_{V_0}^{V_1}p\,dV$ during the emission time t_1.[17] The initial bubble volume is $V_0=L_0A$, where L_0 and A denote the bubble initial width and its cylindrical cross-sectional, area respectively. During the acoustic emission the bubble volume increases to $V_1=L_1A$, where $L_1=L_0+u_st_1$. Since the bubble expands adiabatically, we have

$$e_s = m_0(\varepsilon_0 - \varepsilon_1), \tag{9b}$$

where m_0 is the mass inside the bubble and ε_0, ε_1 are the respective specific energies before and after the acoustic emission process. The acoustic energy is then subtracted from the initial bubble energy to give the available energy for bubble expansion.

After acoustic emission, there is still a process of compressibility, which effectively ends when the acoustic wave reaches a distance on the order of the fiber width. At the final collapse stage of the bubble in the 2D case, there is another episode of acoustic emission. However, most of the bubble energy is dissipated by heating of the close surroundings, and the bubble rebound is usually small. This dissipated energy spreads away from the fiber tip by the induced flow in the ambient fluid.

B. Vapor bubble generated in viscous fluid

In order to include viscosity and surface tension in the model, we need to rewrite Eq. (6). The pressure P at the bubble boundary, instead of being simply the bubble pressure p_b, is now combined with the contributions from viscosity and surface tension.[18–20] The pressure introduced by the surface tension is given by $p_\gamma = -\gamma(1/R_1 + 1/R_2)$, where R_1 and R_2 are the major radii of curvature of the bubble boundary and γ is a constant depending on the properties of the surrounding fluid.[18] For a bubble boundary which, at a given time is defined by $z = f(r)$, a simple procedure yields[21]

$$R_1 = \frac{(1+f'^2)^{3/2}}{f''}, \quad R_2 = \frac{r\sqrt{1+f'^2}}{f'}. \tag{10}$$

These relations hold for an arbitrary body of revolution generated by $z = f(r)$. The first radius R_1, simply represents the curvature of the planar curve $z = f(r)$. For example, if the body of revolution is generated by a straight line, then $f''(r) = 0$ and the radius of curvature is infinite. The second radius of curvature, R_2, is the result of the rotation of the curve $z = f(r)$.

The pressure added by the presence of viscosity is given by $p_\mu = 2\mu(\partial u_n/\partial r_n)$, where $\partial u_n/\partial r_n$, the normal derivative of the velocity component u_n, is evaluated at the bubble's boundary and μ is the viscosity of the soft tissue.[18–20] The pressure at the bubble boundary is thus taken as

$$P = p_b + 2\mu\frac{\partial u_n}{\partial r_n} - \gamma\left(\frac{1}{R_1} + \frac{1}{R_2}\right). \tag{11}$$

In the case of the 1D Rayleigh model, we have $u = UR^2/r^2$, where R and U are, respectively, the bubble radius and velocity (on the boundary). Therefore, $(\partial u/\partial r)_R = -2UR^2/R^3 = -2U/R$, which implies the familiar result $P_\mu = -4\mu U/R$. Since $R_1 = R_2 = R$ as well, we obtain from Eq. (11) $P_\gamma = 2\gamma/R$ as expected.

III. THE NUMERICAL PROCEDURE

At the initial time $t_0 = 0$, we assume that the bubble starts as a cylinder with known radius and layer deposition width L_0 at a given room temperature and initial density ρ_0 inside the bubble. The deposition of energy by a short-pulse laser increases the bubble temperature to T_0 and the two quantities ρ_0, T_0 determine the constant entropy S_0 of the bubble, the initial pressure p_0, and the initial specific energy ε_0. An equation of state (EOS) of water is used, based on NBS steam tables.[22] We use S_0 to obtain the adiabat of the fluid inside the bubble, which provides the pressure as a function of density. A homogeneous adiabatic acoustic emission of $k\%$ from the initial bubble energy ε_0, provides corrected values for the pressure (p_1), temperature (T_1), density (ρ_1), and specific energy (ε_1) at an acoustic emission time t_1. The value of k can be obtained from Eqs. (9a), (9b), and the estimate $t_1 \cong 2L_0/c_s$.

Since the flow potential model does not accurately represent the bubble expansion for very short times, we must determine an initial potential flow time $t_2 > t_1 > t_0$ beyond which our model is valid. This is a characteristic time given by $t_2 \cong 4r_f/c_s$, in which the acoustic wave samples a complete cycle of the fiber cross section. The initial data for the potential flow model at t_2 can be first obtained by applying a 2D hydrodynamic code to the early time evolution of the bubble. Such a simulation includes the geometry of the fiber, the velocity profile along the bubble boundary, and the pressure (p_2), temperature (T_2), density (ρ_2), and specific energy (ε_2). (Note that any one of these thermodynamic quantities together with S_0 determines the others as well.[3]) In Sec. IV B we will show that the conditions at t_2 can be determined by physical considerations independent of the 2D hydrodynamic simulation. This enables us to obtain a solution that is not tied in any way to the hydrodynamic simulations.

In the calculations, we use the unstructured mesh finite-element solver (UMFES), which is a general finite-element solver for 2D elliptic partial differential equations (e.g., Laplace's equation) over an arbitrary bounded domain, with Dirichlet (specified ϕ), homogeneous Neumann $(\partial\phi/\partial n = 0)$ or mixed $[(\partial\phi/\partial n) + \sigma\phi = \eta]$, with σ and η specified on the boundary) boundary conditions.[12,13] The density function of the generated mesh (i.e., of the mesh triangular elements) is supplied by the user.

The validity of the initial geometry and the initial velocity profile at time t_2 at the bubble boundary can be verified using an energy conservation principle. Indeed, by solving Laplace's equation outside the bubble at time t_2, we obtain the potential and velocity of every fluid element and consequently the total kinetic energy e_k of the ambient fluid. Since the energy dissipated during $t_1 < t < t_2$ is small, we have

$$(\varepsilon_1 - \varepsilon_2)m_0 \cong e_k, \tag{12}$$

where m_0 is the mass inside the bubble and $m_0\varepsilon_1 = m_0\varepsilon_0 - e_s$, with e_s being the acoustic energy emitted by Eqs. (9a) and (9b).

The numerical procedure is as follows.

Initial step: Solve Laplace's equation in cylindrical geometry outside the bubble, using the initial velocity profile on the bubble boundary, from the results of a 2D hydrodynamic code at time t_2 or from independent analysis (see Sec. IV C). The initial pressure, temperature, and density inside the bubble are the previously defined p_2, T_2, ρ_2. These quantities are derived from the bubble's dimensions at time t_2 assuming constant entropy S_0. At "infinity," i.e., at boundary

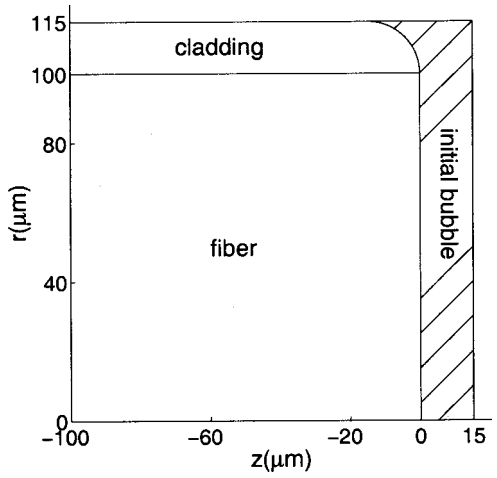

FIG. 1. The initial bubble in cylindrical coordinates *r,z* obtained from 2D hydrodynamic code after 300 ns.

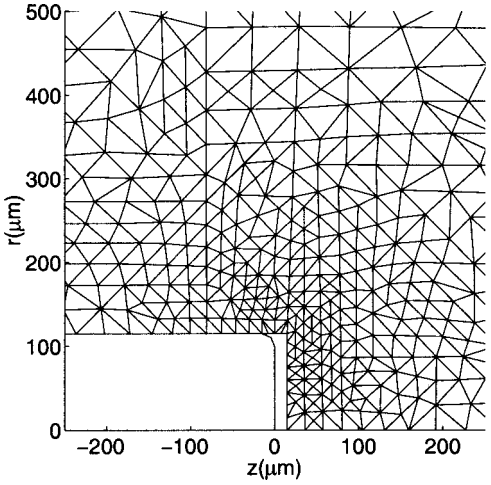

FIG. 3. Triangulation outside the bubble in cylindrical coordinates *r,z*, at $t = 300$ ns.

points far from the fiber tip and the bubble boundary, we assume homogeneous Dirichlet boundary conditions, i.e., $\phi = 0$. Along the surface of the fiber and the problem axis of symmetry, we take a zero normal fluid velocity, i.e., $\partial\phi/\partial n = 0$. At the bubble boundary we update the flow potential after each time step. We thus obtain the flow potential distribution ϕ_2 outside the bubble boundary. On the bubble boundary we denote the flow potential by Φ_2 and the pressure there is simply $P_2 = p_2$.

At the nth time step ($n \geqslant 3$) we perform the following.

Step 1: Use Eq. (6) to update the flow potentials

$$\Phi_n = \Phi_{n-1} + \Delta t_{n-1}\left[\frac{1}{\rho}(P_{n-1} - p_\infty) - \frac{U_{n-1}^2}{2}\right], \tag{13}$$

where P_{n-1} is the bubble effective pressure on the boundary as presented by Eq. (11), ρ the outside fluid density, and Φ_{n-1}, U_{n-1} are the flow potential and velocity at the bubble boundary during the $(n-1)$th time step, respectively.

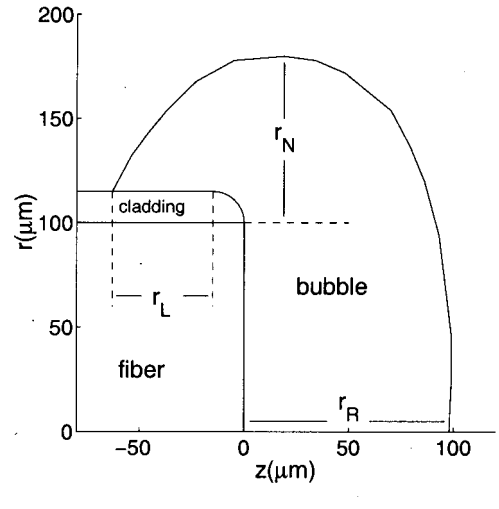

FIG. 4. Defining the bubble's three lengths: r_R, r_N, r_L.

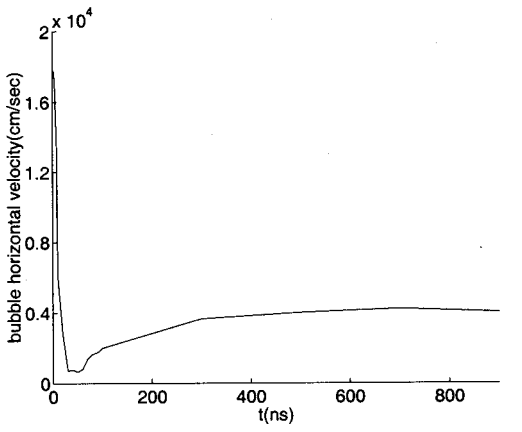

FIG. 2. The bubble horizontal velocity profile calculated by the 2D hydrodynamic code. The potential flow model is valid approximately after 300 ns, when this velocity reaches an asymptotic value of approximately 4000 cm/s.

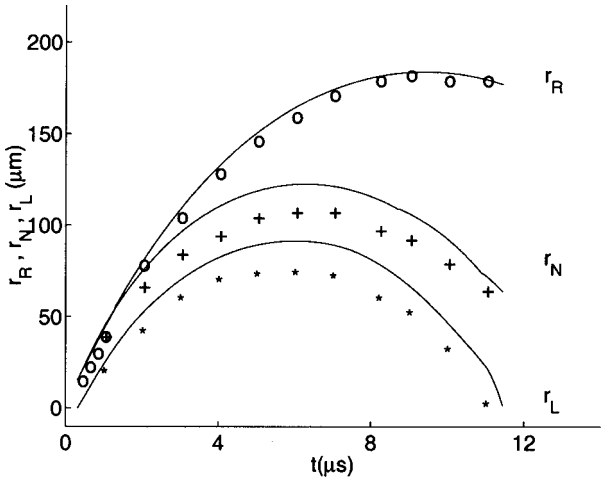

FIG. 5. The bubble's lengths vs time for ambient pressure $p_\infty = 10$ bar: our model (solid lines) compared with 2D hydrodynamic calculations (discrete points: *o*, +,* denote r_R, r_N, r_L, respectively). Initial conditions inside the bubble taken at $t = 300$ ns are: $p_2 = 40$ bar, $T_2 = 249\,^\circ$C, $\rho_2 = 0.33$ g/cm^3; the initial horizontal and normal velocities of the bubble front and upper edge are 4000 cm/s and 0, respectively.

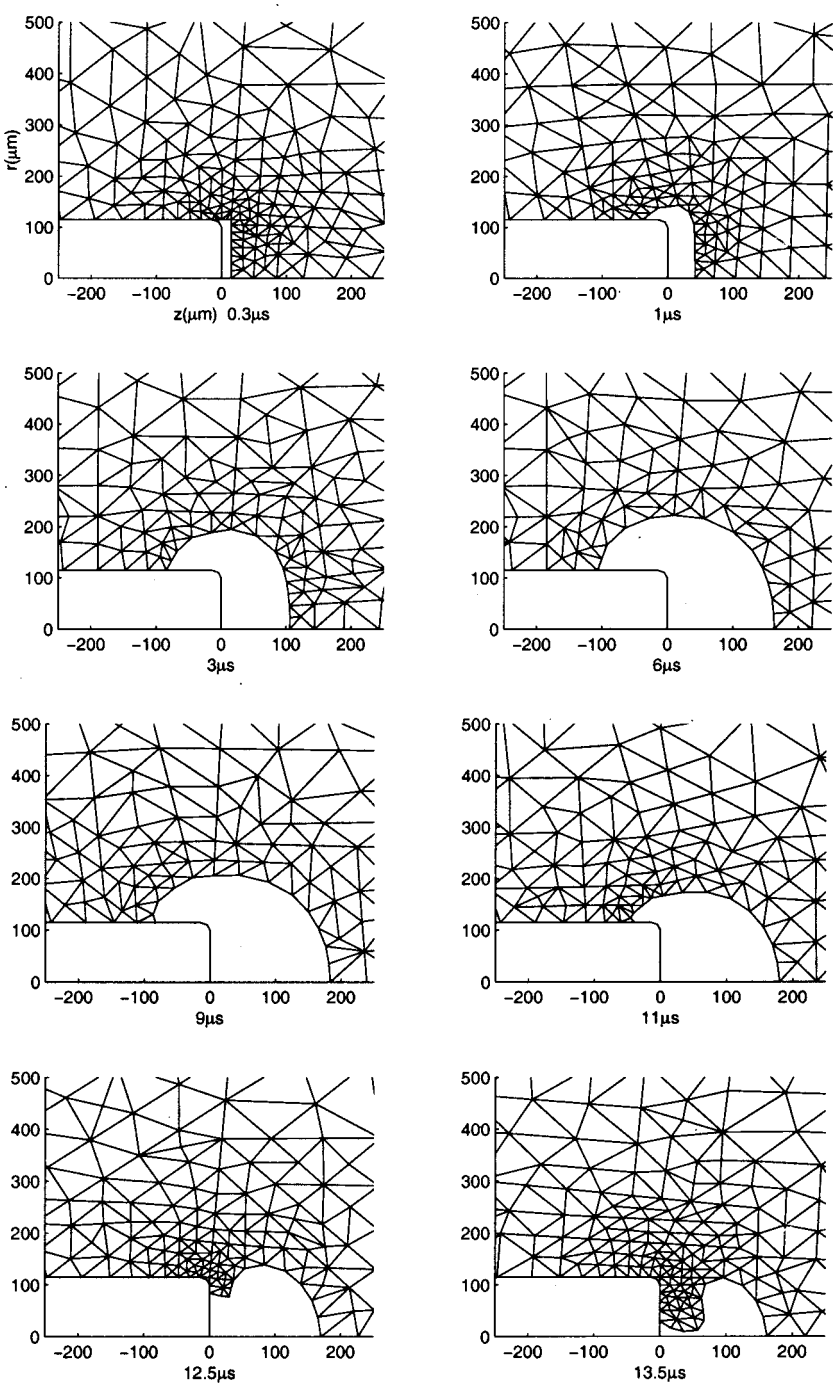

FIG. 6. Bubble expansion and collapse in cylindrical coordinates *r, z* at various times for $p_\infty = 10$ bar; the initial conditions are those of Fig. 1.

Step 2: Solve Laplace equation for ϕ_n outside the region using UMFES; then update the velocities $\mathbf{U}_n$ at the bubble boundary using

$$\mathbf{U}_n = -\nabla \phi_n, \tag{14}$$

where $\nabla \phi_n$ is calculated numerically from ϕ_n. Since ϕ is approximated linearly over each mesh triangle, $\nabla \phi_n$ is constant over each element.

Step 3: Update the bubble boundary using the velocities obtained in step 2 and the time interval Δt_n.

Step 4: Update the bubble density ρ_n by calculating the bubble volume V_n and applying mass conservation

$$\rho_n V_n = \rho_0 V_0. \tag{15}$$

The adiabat of S_0 is used to calculate the new bubble pressure p_n. For the next step we use ρ_n, p_n, $\mathbf{U}_n$ in Eq. (13) to calculate Φ_{n+1}.

IV. RESULTS AND DISCUSSION

Throughout this work we have assumed a fiber of outer radius $r_f = 115\,\mu$m, including 15 μm of cladding and a 100 μm laser core in which the laser beam propagates (see Fig. 1). The upper right-hand corner of the fiber is curved and simulated by a quarter circle of radius 15 μm. We consider a homogeneous laser absorption length of 7 μm and assume the bubble to be initially at room temperature of 17 °C with

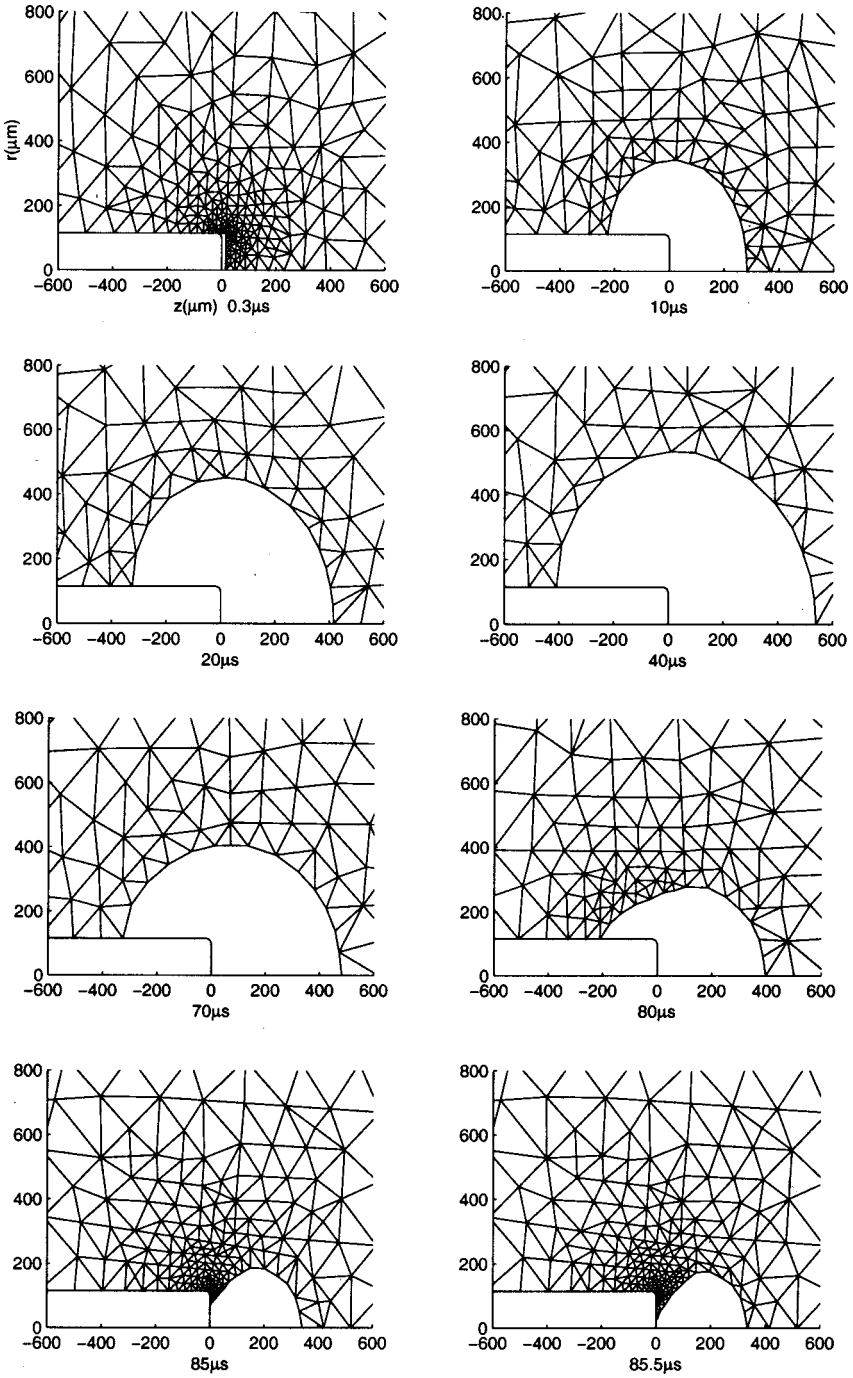

FIG. 7. Bubble expansion and collapse in cylindrical coordinates r, z at various times for $p_\infty = 1$ bar. The initial conditions are those of Fig. 1.

an initial density of $\rho_0 = 0.9989\ \mathrm{g/cm^3}$. During the energy deposition by the laser, the bubble temperature increases to 350 °C. Using the NBS steam tables,[22] we obtain the bubble's entropy $S_0 = 2.897 \times 10^7$ erg/g, which remains constant throughout the whole process. The initial pressure is $p_0 = 6008$ bar and the initial specific energy is $\varepsilon_0 = 1.197 \times 10^{10}$ erg/g. By using Eqs. (9a) and (9b), we can derive an adiabatic acoustic emission of about 5% which lasts about $t_1 = 9$ ns and reduces the bubble energy to a lower value of $\varepsilon_1 = 1.136 \times 10^{10}$ erg/g. Consequently, using the NBS steam tables and the adiabatic nature of the process, we find that the initial temperature, density, and pressure become $T_1 = 262\,^\circ\mathrm{C}$, $\rho_1 = 0.78\ \mathrm{g/cm^3}$, $p_1 = 74$ bar, respectively. The drop in density causes the bubble width to increase from 7 to 8.8 μm.

Since the flow potential model is not valid at the very early stage of the bubble expansion, we first use a 2D hydrodynamic code to obtain the bubble geometry and the bubble boundary velocity after $t_2 = 300$ ns. At this time the bubble two-dimensional projection (approximately) maintains a rectangular shape with length 115 μm and width 15 μm and expands to the upper edge of the fiber's curved corner (Fig. 1). The z component of velocity of the bubble as obtained from the 2D hydrodynamic code is illustrated in Fig. 2. It

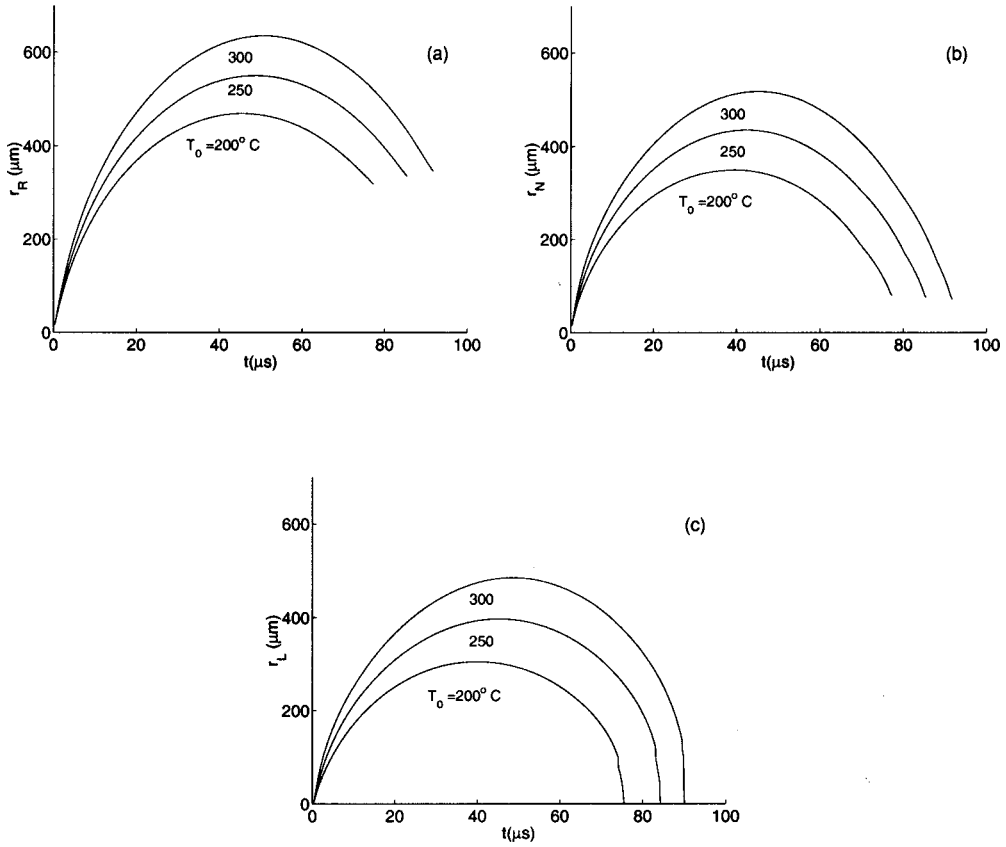

FIG. 8. The bubble's lengths vs time for ambient pressure $p_\infty = 1$ bar and initial temperatures $T_0 = 200\,°\text{C}$, 250 °C, 300 °C.

varies very slowly in the time interval $0.3\,\mu\text{s} < t < 1\,\mu\text{s}$ and reaches an asymptotic value of 4000 cm/s. This asymptotic velocity is also approximately the value calculated by a 2D hydrodynamic code for the normal velocity at the top ($r = r_f$) of the initial bubble. The normal velocity, however, which pertains to the bubble's short dimension, is less relevant to the overall expansion of the bubble. Varying the value of this velocity between zero and 4000 cm/s turns out to have little effect on the global solution. The initial conditions obtained for this geometry after 300 ns are $T_2 = 249\,°\text{C}$, $\rho_2 = 0.33\,\text{g/cm}^3$, $p_2 = 40\,\text{bar}$, and $\varepsilon_2 = 1.127 \times 10^{10}\,\text{erg/g}$. A typical triangulation for a free boundary problem where the density function of the elements depends inversely on the distance from the fiber's tip, is shown in Fig. 3.

As illustrated in Fig. 4, for a typical time step, three characteristic lengths of the bubble are defined: r_R denotes the distance between the right front midpoint of the bubble and its left rear, r_N is the distance between the highest point of the bubble boundary and the bottom of the cladding, and r_L is the distance between the bubble's leftmost point on the cladding and the left edge of the fiber's curved corner. At the beginning, i.e., for $t = 300$ ns, we have $r_R = 15\,\mu\text{m}$, $r_N = 15\,\mu\text{m}$, $r_L = 0\,\mu\text{m}$.

A. Numerical results for water

We considered two cases of ambient pressures $p_\infty = 1$, 10 bar for an aqueous system.

1. Case 1: $p_\infty = 10$ bar

Since the detailed hydrodynamic calculation is very time consuming, it is more convenient to provide a comparison for a shorter time scale evolution in the case $p_\infty = 10$ bar rather than in the case $p_\infty = 1$ bar.

We have utilized the LATIS (Laser TISsue) program[2] to provide initial conditions for the 2D Rayleigh model and to compare with the results at later times. LATIS is a general-purpose program for modeling laser–tissue interactions. In addition to other processes important in laser–tissue interaction, LATIS solves the time-dependent compressible fluid equations in 2D cylindrical symmetry using a Lagrangian finite difference numerical method.[2] LATIS, which uses the same equation of state as the 2D Rayleigh model, has been previously verified against experimental data.[3]

In Fig. 5 we compare the bubble's three radii computed by our flow potential model with those obtained using LATIS. The initial normal velocity is zero, a value that provided the best agreement with the 2D hydrodynamic computations. However, as previously stated, little change has been observed for an initial normal velocity of 4000 cm/s. The choice of the initial velocity profile was consistent with the energy conservation principle [Eq. (12)]. In the case illustrated in Fig. 5 we get $(\varepsilon_1 - \varepsilon_2) m_0 = 20\,\text{erg}$, which is in agreement with the simulated fluid kinetic energy $e_k = 22\,\text{erg}$, calculated from the flow potential by integrating $|\nabla \phi|^2$ outside the bubble at $t = 300$ ns.

The maximum values of r_L, r_N, r_R are 91, 123, and 184

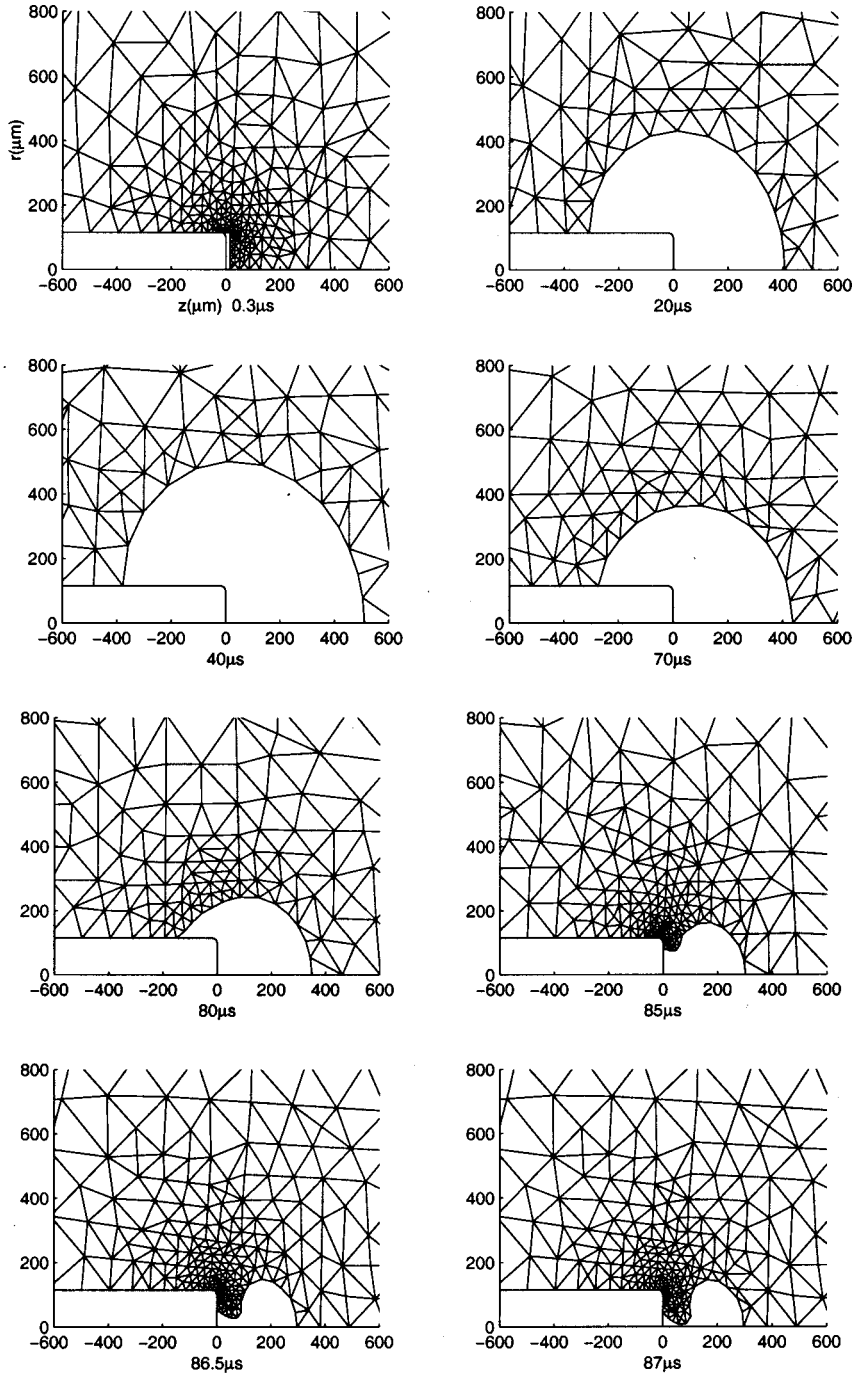

FIG. 9. Bubble expansion and collapse in cylindrical coordinates for $p_\infty = 1$ bar, viscosity coefficient $\mu = 1.35$ poise, and surface tension coefficient $\gamma = 54$ erg/cm^2.

μm and are obtained at times of 5.8, 6.1, and 9.1 μs, respectively. The results for r_R were in very good agreement with those obtained by the hydrodynamic code. Good agreement was also received for r_L and r_N except at about the maximum expansion point, where deviation up to 15% from the detailed hydrodynamic computations was observed. The global expansion collapse process of the bubble is shown in Fig. 6. Towards the end of the collapse phase, the bubble collapses away from the fiber as observed in experiment as well.[14]

2. Case 2: $p_\infty = 1$ bar

The physical conditions that exist in practical problems usually suggest an ambient pressure of about $p_\infty = 1$ bar. We therefore applied our method to this case as well, a case for which the detailed 2D hydrodynamic calculation is prohibitively time consuming. The initial conditions at the short time of 300 ns can be chosen to be the same as in case 1. The maximum values of the radii r_L, r_N, r_R are obtained 398, 435, and 551 μm and are attained at 45, 42, and 49 μs, respectively. The global expansion collapse process is shown in Fig. 7. At the beginning of the process the pressure inside the bubble is dominant and there is hardly any difference between the two cases. Later, the lower ambient pressure becomes significant, and this causes a sizable increase in the time of expansion and collapse and of the bubble's dimensions, compared to the 10 bar case.

During the ellipsoidal-shaped collapse, as seen for ex-

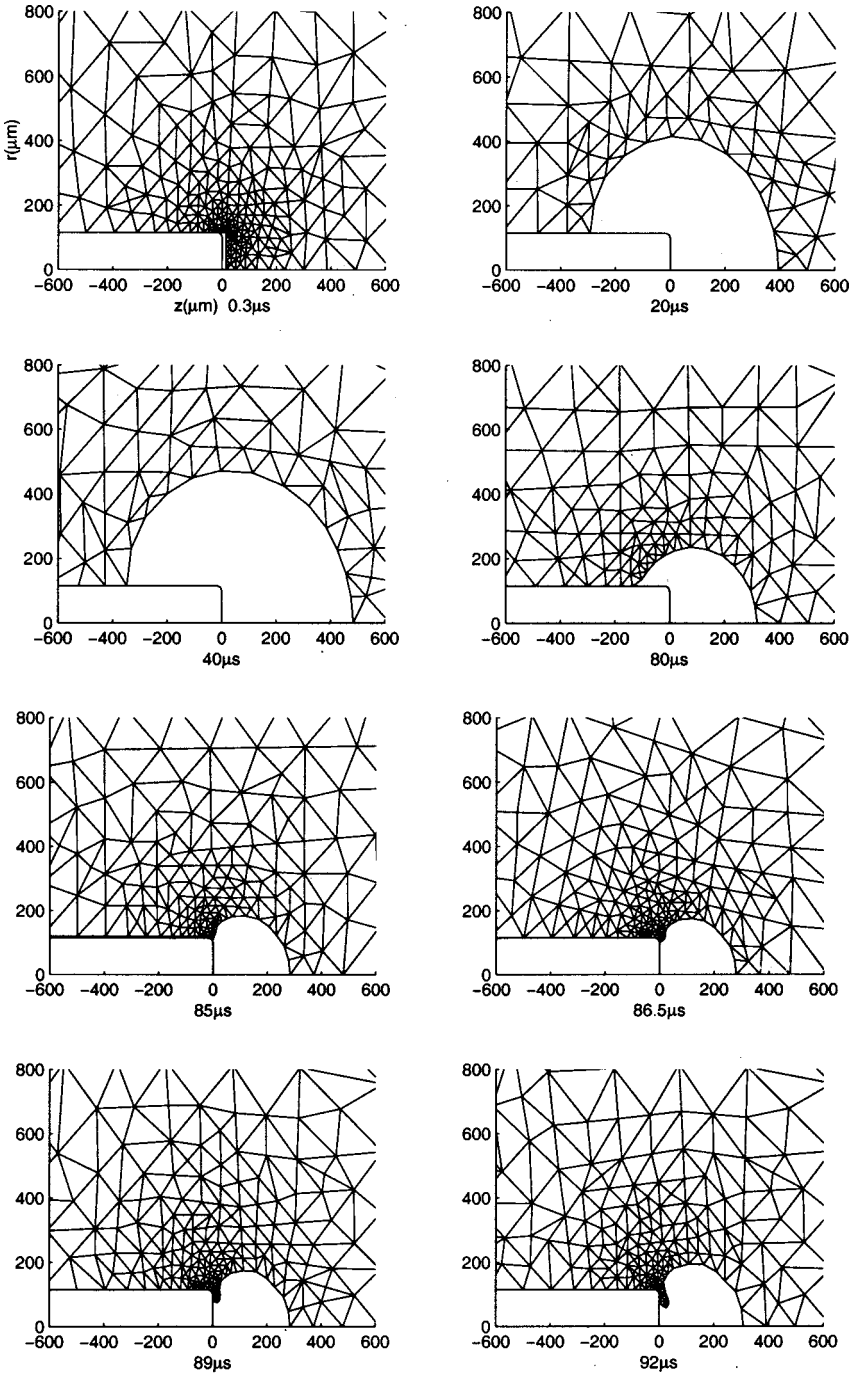

FIG. 10. Bubble expansion and collapse in cylindrical coordinates for $p_\infty = 1$ bar, viscosity coefficient $\mu = 2.7$ poise, and surface tension coefficient $\gamma = 54$ erg/cm^2.

ample in the last frame of Fig. 7, the liquid forms a jet directed away from the fiber.[23] Jet formation and bubble collapse near a rigid material or elastic boundary such as biological tissue may cause material erosion and collateral damage.[23] Mechanisms such as jet penetration and jet-like ejection of boundary material, elastic rebound of the boundary, and tensile stresses from the collapsing bubble, cause enhanced ablation of the surrounding material and damage.

We also studied the sensitivity of the bubble dynamics to the initial temperature. This is presented in Fig. 8, where results for $T_0 = 200\,^\circ$C, 250 °C, and 300 °C show significant increase of the bubble's dimensions with temperature.

B. Numerical results for viscous fluid

In the following cases we took $p_\infty = 1$ bar and assumed various nonzero viscosity and surface tension coefficients which are typical of gelatin-type soft tissues. As baseline values, we took $\mu = 1.35$ poise and $\gamma = 54$ erg/cm^2.[24] The global expansion and collapse process is given in Fig. 9. The maximum bubble size is somewhat smaller than in Fig. 7, where viscosity and surface tension are not included. The main difference between the two cases is that in the presence of viscosity the bubble collapses later in time and its detachment from the fiber occurs further away. A case with in-

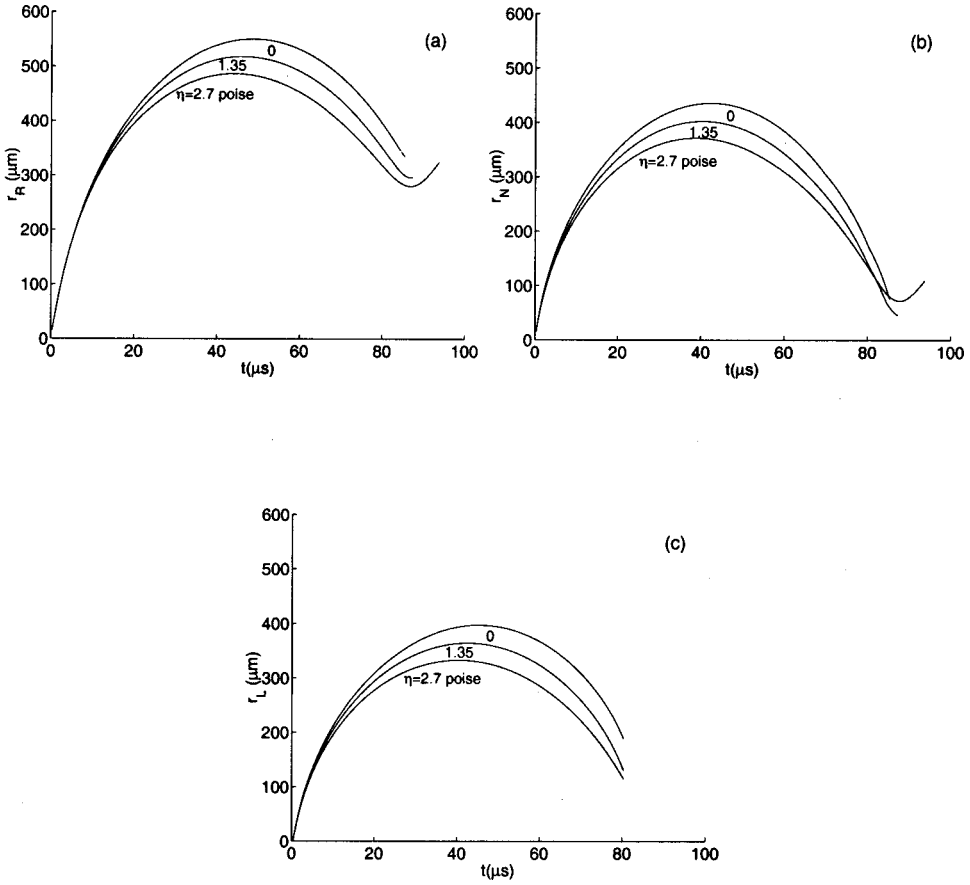

FIG. 11. Sensitivity to viscosity coefficient bubble's lengths vs time for $p_\infty = 1$ bar, $\mu = 0$, 1.35, 2.7 poise, and $\gamma = 54$ erg/cm^2.

creased viscosity, $\mu = 2.7$ poise, is shown in Fig. 10. Here, the collapse is further delayed but ends before separation occurs and the bubble is again expanding. The sensitivity of the bubble's dimensions to the viscosity coefficient is presented in Fig. 11. A soft tissue with larger viscosity clearly reduces the bubble's dimensions.

The velocity profile, which is very helpful in understanding the collapse process, is given for $p_\infty = 1$ bar, $\mu = 1.35$ poise, and $\gamma = 54$ erg/cm^2 in Fig. 12. During the collapse, we observe a large velocity field generated near the fiber tip and aimed away from the fiber towards the bubble center. A jet is formed towards the right and pushes the liquid away from the fiber.

C. Disengagement from the hydrodynamic code

The potential flow model, which is valid throughout most of the bubble expansion collapse process, is determined by the initial velocity of the bubble boundary and by the initial bubble geometry. It is possible to approximate the initial frontal velocity using physical considerations such as an energy conservation principle as given in Eq. (12), where the normal velocity is taken as zero. Exact knowledge of the bubble's initial dimensions is of less significance. In fact, the global expansion and collapse processes for different geometries are very similar, provided that the initial bubble dimensions are similar. In the case of $p_\infty = 10$ bar we calculated the process over a period of 12 μs for bubble initial widths of 10, 15, and 20 μm, as presented in Fig. 13. For each problem we calculated the bubble density, pressure, and temperature, assuming an adiabatic process, and using Eq. (12) obtained a similar initial frontal velocity of approximately 4000 cm/s. The associated bubble lengths as functions of time are illustrated in Fig. 13, which demonstrates the insensitivity of the process to the initial geometry.

Since in most applications one is mainly interested in the approximate bubble geometry during the global expansion process, our procedure can be disengaged from the detailed 2D hydrodynamic code. It is sufficient to start with a reasonable initial bubble width and a frontal initial velocity for which Eq. (12) holds. For example, let us assume a potential flow model after $t_2 = 300$ ns. This value for t_2 can be obtained as the time in which the acoustic wave samples a complete cycle of the fiber cross section, for example $t_2 \cong 4r_f/c_s \cong 300$ ns. It can also be verified by the hydrodynamic code (Fig. 2) as the time where the bubble horizontal velocity enters the asymptotic zone of about $u_2 = 4000$ cm/s. By virtue of Eq. (12) and the relation $L_2 = L_0 + u_2 t_2$ for the bubble width, we get a self-consistent horizontal initial velocity of about 4000 cm/s. Since the initial bubble width at $t_0 = 0$ is $L_0 = 7$ μm, the bubble width at $t_2 = 300$ ns is $L_2 = 19$ μm. This value falls inside the interval $10\ \mu\text{m} \leqslant L_2 \leqslant 20\ \mu\text{m}$, which we tested and illustrated in Fig. 13.

There is a fundamental difference between the current 2D flow potential model and the 1D spherical Rayleigh model, necessitating the implementation of the initial conditions at a later time (t_2) in the 2D case. In the examples explored in this paper, the heated region of fluid is shaped

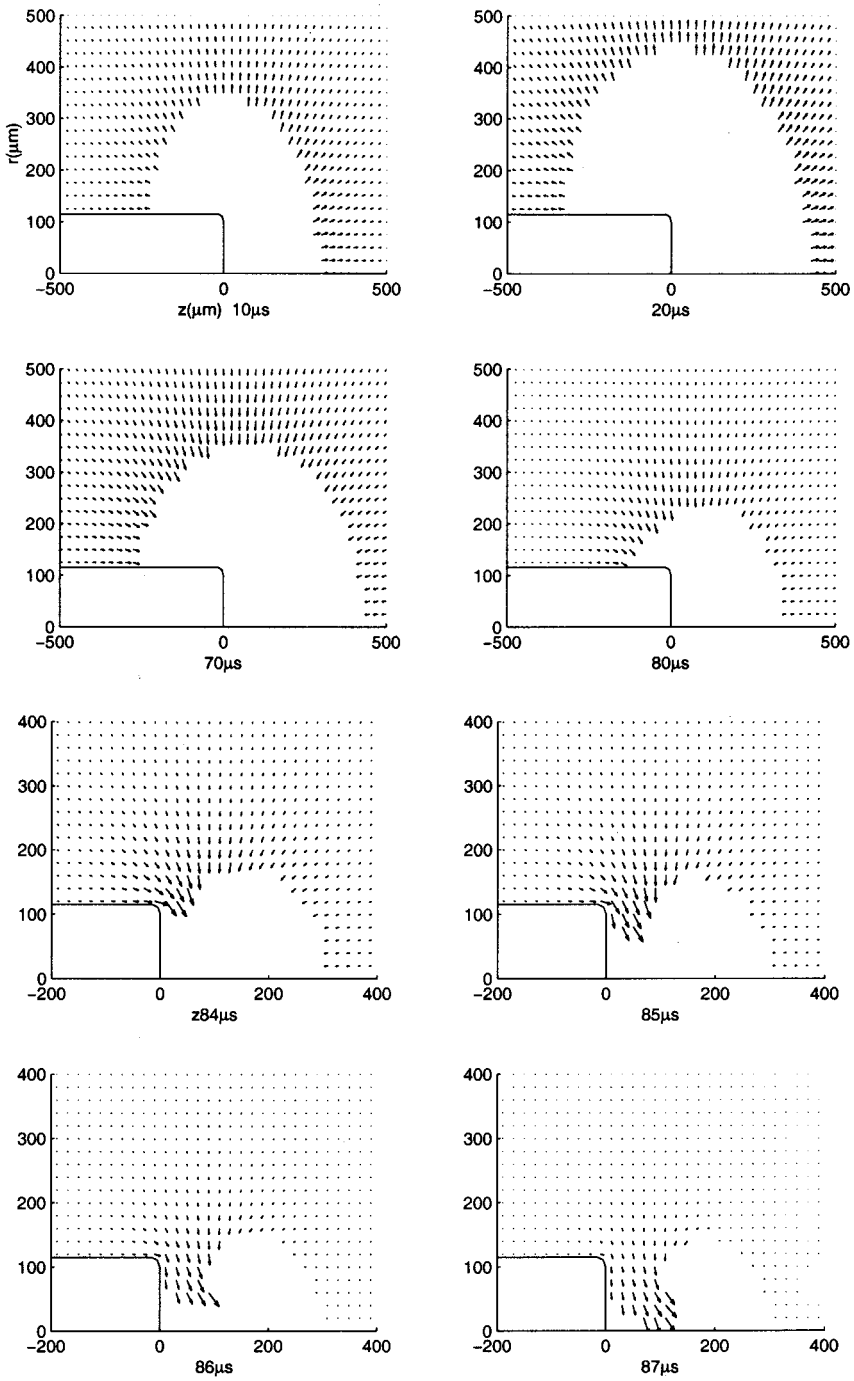

FIG. 12. Velocity profiles throughout bubble expansion and collapse for $p_\infty = 1$ bar, $\mu = 1.35$ poise, and $\gamma = 54$ erg/cm^2.

like a very thin pancake whose thickness is much smaller than its radius. Therefore, the dynamics begins to evolve much like a 1D heated slab. However, there is no bubble formation for a 1D slab in the incompressible fluid approximation, since the velocity is constant with distance from the source. It is only after sound waves have traveled to the outer radius of the heated pancake that a radial flow can begin from which a bubble is formed. Thus, the 2D case requires a long time to set up the flow needed to form a bubble. The case is much simpler in 1D spherical geometry, where the bubble begins to form as soon as the sound waves cross the thickness of the heated regions, thereby circumventing the need for a t_2 time scale introduced earlier. The divergence of the flow and the associated $1/r^2$ velocity field allow this early bubble formation.

V. SUMMARY

A potential flow method was applied to obtain a 2D Rayleigh-type model for bubble expansion and collapse. The model includes viscosity and surface tension terms and can thus realistically treat bubble evolution within a real soft tissue. The main assumption was that the inside of the bubble is homogeneous in pressure and density, as is usually assumed in a Rayleigh model. The procedure derives the initial conditions for the potential flow model at time t_2 either from

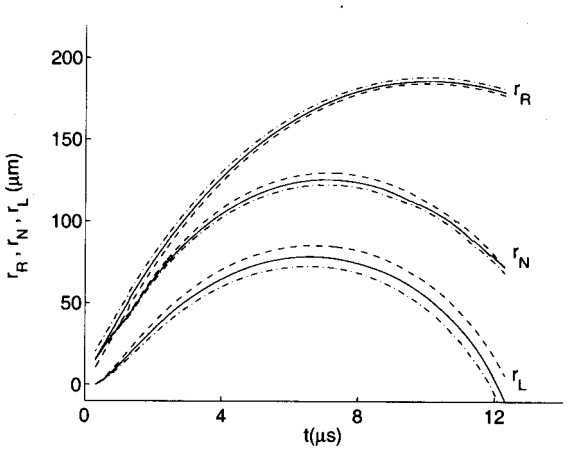

FIG. 13. The bubble's lengths vs time for ambient pressure $p_\infty = 10$ bar and several initial widths: 10 μm (dashed), 15 μm (solid), and 20 μm (dash-dot).

physical considerations such as energy conservation, or from a detailed 2D hydrodynamic simulation run during a short time scale t_2. These conditions include the initial geometry and velocity profile at the bubble boundary, which can be validated using an energy conservation principle. The numerical scheme consists of solving Laplace's equation for the flow potential outside the bubble, subject to a moving boundary condition on the bubble boundary. The 1D Rayleigh bubble expansion is a special case of our 2D model. We used a general high-order finite-element solver for 2D elliptic problems, which provided our model with the flexibility to treat various tissue boundary conditions and geometries.

The 2D Rayleigh type model presented in this work, which is faster and simpler than a 2D compressible hydrodynamic simulation, can be applied to the design and understanding of fiber-based medical therapies. It can also be extended to include other physical mechanisms that can affect tissue behavior such as strength and failure properties.

ACKNOWLEDGMENTS

Part of this work was performed under the auspices of the U.S. Department of Energy by the University of California Lawrence Livermore National Laboratory under Contract No. W-7405-ENG-48.

[1]K. W. Gregory, "Laser thrombolysis," in *Interventional Cardiology*, edited by E. J. Topol (Sanders, New York, 1994), p. 892; A. Vogel, S. Busch, K. Jungnickel, and R. Birngruber, "Mechanisms of intraocular photodisruption with picosecond and nanosecond laser pulses," Lasers Surg. Med. **15**, 32 (1994); T. G. van Leeuwen, E. D. Jansen, M. Motamedi, C. Borst, and A. J. Welch, "Pulsed laser ablation in soft tissue," in *Optical-Thermal Response of Laser Irradiated Tissue*, edited by A. J. Welch and M. J. C. Van Gemert (Plenum, New York, 1995), p. 709; A. Vogel, R. Engelhardt, U. Behnle, and U. Parlitz, "Minimization of cavitation effects in pulsed laser ablation illustrated on laser angioplasty," Appl. Phys. B: Photophys. Laser Chem. **62**, 173 (1996); A. Vogel, S. Busch, and U. Parlitz, "Shock wave emission and cavitation bubble generation by picosecond and nanosecond optical breakdown in water," J. Acoust. Soc. Am. **100**, 148 (1996); U. Sathyam, A. Shearin, and S. Prahl, "Visualization of microsecond laser ablation of porcine clot and gelatin under a clear liquid," Proc. SPIE **2671**, 28 (1996); M. Strauss, P. A. Amendt, R. A. London, D. J. Maitland, M. E. Glinsky, C. P. Lin, and M. W. Kelly, "Computational modeling of stress transient and bubble evolution in short-pulse laser irradiated melanosome particles," *ibid.* **2975**, 261 (1997); E. J. Chapyak and R. P. Godwin, "Physical mechanisms of importance to laser thrombolysis," *ibid.* **3245**, 12 (1998).

[2]R. A. London, M. E. Glinsky, G. B. Zimmerman, D. S. Bailey, D. C. Eder, and S. L. Jacques, "Laser–tissue interaction modeling with LATIS," Appl. Opt. **36**, 9068 (1997).

[3]P. A. Amendt, R. A. London, M. Strauss, M. E. Glinsky, D. J. Maitland, P. M. Celliers, S. R. Visuri, D. S. Bailey, D. A. Young, D. Ho, C. P. Lin, and M. W. Kelly, "Simulation studies of vapor bubble generation by short-pulse laser," in *Laser–Tissue Interaction, Tissue Optics, and Laser Welding III*, Proc. SPIE **3195**, 259 (1998).

[4]M. E. Glinsky, P. A. Amendt, D. S. Bailey, R. A. London, A. M. Rubenchik, and M. Strauss, "An extended Rayleigh model of bubble evolution," Phys. Fluids **13**, 20 (2001).

[5]Lord Rayleigh, "On the pressure developed in a liquid on the collapse of a spherical bubble," Philos. Mag. **34**, 94 (1917); M. Plesset, "The dynamics of cavitation bubbles," J. Appl. Mech. **16**, 277 (1949); F. R. Gilmore, "The growth and collapse of a spherical bubble in a viscous compressible liquid," California Institute of Technology, Hydrodynamics Laboratory Report No. 26-4, 1950; R. Hickling and M. S. Plesset, "Collapse and rebound of a spherical bubble in water," Phys. Fluids **7**, 7 (1964); M. S. Plesset and A. Prosperetti, "Bubble dynamics and cavitation," Annu. Rev. Fluid Mech. **9**, 145 (1977); W. Lauterborn, "Numerical investigation of nonlinear oscillations of gas bubbles in liquids," J. Acoust. Soc. Am. **59**, 283 (1976); W. Lauterborn and U. Parlitz, "Methods of chaos physics and their application to acoustics," *ibid.* **84**, 1975 (1988); C. E. Brennen, *Cavitation and Bubble Dynamics* (Oxford University Press, Oxford, 1995).

[6]R. T. Knapp, J. W. Daily, and F. G. Hammitt, *Cavitation* (McGraw-Hill, New York, 1966), p. 94.

[7]L. D. Landau and E. M. Lifshitz, *Fluid Mechanics* (Pergamon, New York, 1987), pp. 1–43, 251–312.

[8]M. S. Plesset and R. B. Chapman, "Collapse of an initially spherical vapor cavity in the neighborhood of a solid boundary," J. Fluid Mech. **47**, 283 (1971).

[9]A. Prosperetti and J. W. Jacobs, "A numerical method for potential flows with a free surface," J. Comput. Phys. **51**, 365 (1983).

[10]J. R. Blake and D. C. Gibson, "Growth and collapse of a vapor cavity near a free surface," J. Fluid Mech. **111**, 123 (1981).

[11]J. R. Blake, B. B. Taib, and G. Doherty, "Transient cavities near boundaries: Part 1. Rigid boundary," J. Fluid Mech. **170**, 479 (1986).

[12]M. Friedman and A. Kandel, "On the design of fuzzy intelligent differential equation solver," in *Fuzzy Expert Systems*, edited by A. Kandel (CRC, Boca Raton, 1994).

[13]M. Friedman and A. Kandel, *Fundamentals of Computer Numerical Analysis* (CRC, Boca Raton, 1994), pp. 448–450, 519.

[14]P. Celliers, L. Da Silva, N. J. Heredia, B. M. Mammini, R. A. London, and M. Strauss, "Dynamics of laser-induced transients produced by nanosecond duration pulses," Proc. SPIE **2671**, 22 (1996).

[15]E. J. Chapyak and R. P. Godwin, "Comparison of numerical simulations and laboratory studies of shock waves and cavitation bubble growth," Proc. SPIE **2975**, 335 (1997).

[16]M. Strauss, P. A. Amendt, R. A. London, D. J. Maitland, M. E. Glinsky, P. Celliers, D. S. Bailey, D. A. Young, and S. L. Jacques, "Computational modeling of laser thrombolysis for stroke treatment," Proc. SPIE **2671**, 11 (1996).

[17]G. Paltauf and H. Schmidt-Kleiber, "Model study to investigate the contribution of spallation to pulsed laser ablation of tissue," Lasers Surg. Med. **16**, 277 (1995).

[18]L. D. Landau and E. M. Lifshitz, *Fluid Mechanics* (Pergamon, New York, 1987), pp. 48–49, 238–239.

[19]R. T. Knapp, J. W. Daily, and F. G. Hammitt, *Cavitation* (McGraw-Hill, New York, 1966), p. 110.

[20]C. E. Brennen, *Cavitation and Bubble Dynamics* (Oxford University Press, Oxford, 1995), pp. 36–37.

[21]M. Lipschutz, *Differential Geometry*, Schaum's Outline Series (McGraw-Hill, New York, 1969), pp. 181–182.

[22]L. Haar, J. S. Gallagher, and G. S. Kell, *NBS/NRC Steam Tables* (McGraw-Hill, New York, 1984).

[23]R. B. Chapman and M. S. Plesset, "Non-linear effects in the collapse of a

nearly spherical cavity in a liquid,'' Trans. ASME, J. Basic Eng. **94**, 142 (1972); W. Lauterborn, ''Cavitation bubble dynamics—new tools for an intricate problem,'' Appl. Sci. Res. **38**, 165 (1982); E. A. Brujan, K. Nahen, P. Schmidt, and A. Vogel, ''Dynamics of laser-induced cavitation bubbles near an elastic boundary,'' J. Fluid Mech. **433**, 251 (2001); ''Dynamics of laser-induced cavitation bubbles near elastic boundaries: Influence of the elastic modulus,'' *ibid.* **433**, 283 (2001).

[24]G. Paltauf and H. Schmidt-Kleiber, ''Microcavity dynamics during laser-induced spallation of liquids and gels,'' Appl. Phys. A: Mater. Sci. Process. **62**, 307 (1996).